# Section 1
# PROGRESS IN LASER FUSION

## 1.A Electron Kinetics in Laser-Driven Inertial Confinement Fusion

One important requirement for the modeling of the dynamics of laser-driven inertial confinement fusion (ICF) is a proper understanding of electron transport.[1] Electron transport from the critical surface, where most of the laser energy is absorbed, to the cold overdense plasma gives rise to the ablatively driven implosion necessary for fusion. The presence of lateral transport is responsible for smoothing out short-scale thermal modulations that may arise as a result of nonuniform laser illumination, thereby reducing the "seed" for instabilities that are detrimental to efficient target compression.

All processes associated with thermal electron transport are normally studied by solving the fluid equations using classical heat conduction $q_c = -\kappa_c \nabla T$, where $\kappa_c$ is the thermal conductivity (also known as the Spitzer-Härm conductivity),[2] and $T$ is the temperature in energy units. However, typical laser plasmas involve high temperatures and short scale lengths, where the mean free path of a heat-carrying electron (which has an energy of about $7T$) may be comparable to $l = T/|\nabla T|$.[3] Under such conditions the electron transport becomes nonlocal, i.e., cannot be adequately described in terms of a local $\nabla T$, and fluid theory breaks down. The need for a kinetic treatment of the electrons has thus resulted in many transport studies based on numerical solutions of the Fokker-Planck (FP) equation.[4–6] Figure 42.1 schematically shows the consequences of highly nonlocal transport in a laser-produced plasma.

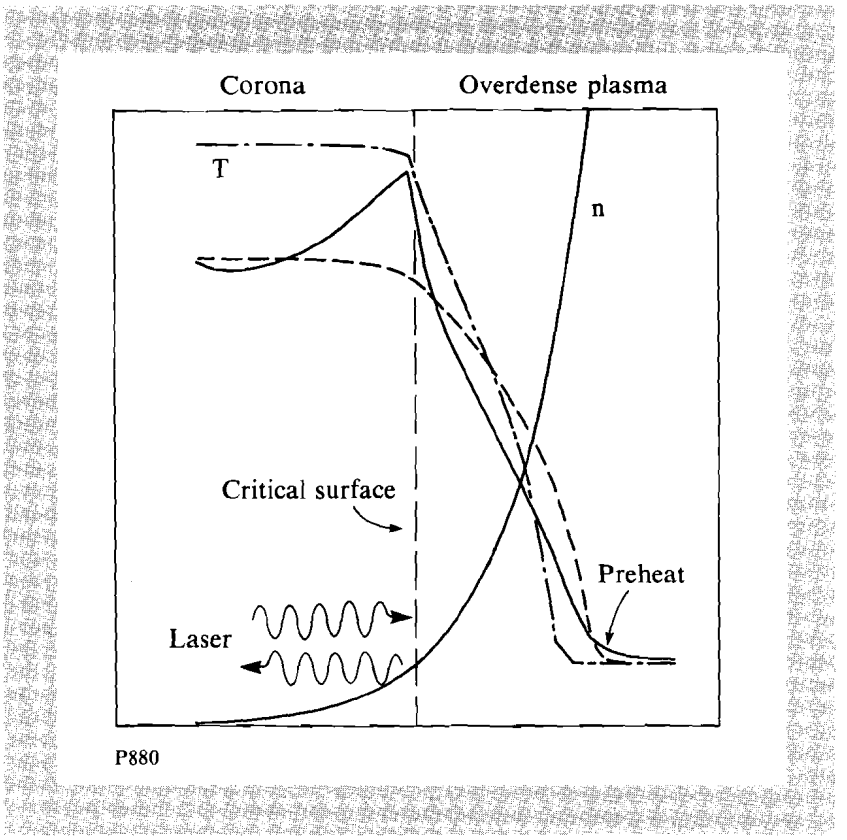


Fig. 42.1
Schematic of density ($n$) and temperature ($T$) profiles in a laser-produced plasma where kinetic effects are assumed dominant. Solid curves refer to FP heat flow, dashed curves to classical heat flow, and dash-dotted curves to flux-limited heat flow. For simplicity, $n$ is assumed invariant.

A characteristic feature of nonlocal transport is the ability of coronal electrons to deposit their energy ahead of the main heat front, thereby causing undesirable preheating of the fuel. Also, if electron thermalization is not sufficiently strong to maintain a Maxwellian distribution, the hot corona becomes partially depleted of heat-carrying electrons. This has the effect of reducing their phase-space density gradient, which in turn reduces their diffusive flow, thereby lowering the effective heat flow. This phenomenon, known as flux inhibition, is commonly identified with a flux-limiting parameter $f$, which when multiplied by the "free-streaming" heat flux

$$q_f = nmv_t^3 (\text{where } v_t = \sqrt{T/m})$$

provides an upper bound to $q_c$.[7] The resultant heat front is correspondingly modified as shown qualitatively in Fig. 42.1. Another manifestation of the departure from classical heat flow arises in multidimensional transport where $\boldsymbol{q}$ is not necessarily parallel to $-\nabla T$.[5,6]

These issues and others associated with nonlocal transport in ICF are addressed in this article. Our main approach is based on comparisons between fluid and FP results. For a review of experimental investigations of heat transport we refer to an article by Delettrez (1986).[8] Other physical processes that may also affect the heat flow, such as magnetic field generation, ion-acoustic instability, and strong inverse-bremsstrahlung heating, are

reviewed by Kruer (1988).[9] In the following sections we first present a brief derivation of the classical heat-flow formula, identify several reasons for its breakdown, and discuss the physical motivation behind the flux limiter. We then provide a more detailed analysis of nonlocal transport by solving the FP equation. In particular we demonstrate a case where the simple flux limiter fails. This is followed by a section devoted to simulations more closely applicable to ICF conditions. We close by discussing the results and what further investigations are needed on the subject of nonlocal transport.

All of the transport simulations presented in this article are obtained using the 2-D FP code SPARK.[5,6] The code is Eulerian (in Cartesian or cylindrical geometries) and is coupled to a fluid-ion package. Magnetic field effects are not presently included.

## Classical Heat Flow and the Flux Limiter

We start with the electron FP equation for a fully ionized plasma, where ions are assumed to be cold and at rest and magnetic-field effects are neglected:

$$\frac{\partial}{\partial t} f + \boldsymbol{v} \cdot \nabla f - \frac{e}{m} \boldsymbol{E} \cdot \nabla_v f = C. \tag{1}$$

The electron distribution function at a spatial point $\boldsymbol{r}$, velocity $\boldsymbol{v}$, and time $t$ is given by $f(\boldsymbol{r},\boldsymbol{v},t)$, $e$ is the electron charge, $m$ is the electron mass, $\boldsymbol{E}$ is the electric field, and $C$ is the FP collision operator. The properties and form of the latter are described in detail elsewhere.[10]

The basis for calculating the heat flow from Eq. (1) assumes that the plasma is close to thermodynamic equilibrium, so that we may expand $f$ as[10]

$$f = f_0 + \boldsymbol{v} \cdot \boldsymbol{f}_1 / v, \tag{2}$$

where $f_0(\boldsymbol{r},v,t)$ is the isotropic part, taken to be a Maxwellian, and $\boldsymbol{f}_1$ is the anisotropic part describing the transport. Substituting Eq. (2) into Eq. (1) and dropping the time derivative we obtain

$$\boldsymbol{f}_1 = -\lambda(v)\left(\nabla f_0 - \frac{e\boldsymbol{E}}{mv}\frac{\partial}{\partial v} f_0\right), \tag{3}$$

where $\lambda(v) = v^4/[n(Z+1)\,4\pi(e^2/m)^2 \ln\Lambda]$ is the velocity-dependent scattering mean free path. In deriving Eq. (3) we have neglected electron-electron momentum exchange, an assumption that is strictly valid only for high-$Z$ plasmas. However, for the purpose of comparing classical with nonlocal transport, this assumption is relatively unimportant.[4]

By invoking quasi-neutrality and therefore zero current [i.e., $j = -(4\pi/3)\int dv v^3 f_1 = 0$] we obtain

$$eE/m = -v_t^2(5\nabla T/2T + \nabla n/n)$$

and

$$f_1 = \lambda_t\left(\frac{v}{v_t}\right)^4\left[\frac{1}{2}\left(\frac{v}{v_t}\right)^2 - 4\right]\frac{\nabla T}{T}f_0, \tag{4}$$

where $\lambda_t = \lambda(v_t)$. We now calculate the heat flow using the definition

$$q = (2\pi/3)\int dv v^4 f_1$$

and obtain $q_c = -\kappa_c \nabla T$, where $\kappa_c = \gamma n v_t \lambda_t$, and $\gamma = 64(2/\pi)^{1/2}$. A more detailed calculation of transport coefficients for arbitrary $Z$ and magnetic fields is given by Epperlein and Haines (1986).[11]

The first problem with the present calculation for $q$ is the fact that the perturbation analysis breaks down, i.e., $|f_1/f_0| \gg 1$, for large $v$, thus giving rise to a negative distribution function. This unphysical behavior is most likely to occur for small values of $l\,(=T/|\nabla T|)$, as seen from Eq. (4). More precisely, since the main contribution to the heat-flow integral comes from $v \sim v^* = 3.7\,v_t$, the validity criterion becomes $\lambda_t < 0.002\,l$, by requiring that $|f_1/f_0| < 1$ at $v^*$.[3,4,12] However, as will be demonstrated in the next section, a more accurate criterion should also involve the electron-electron energy-loss mean free path.

Another limitation of the classical heat-flow formulation comes from the prediction of infinite energy flux as $l \to 0$. On physical grounds we might expect the energy flow to be limited to some fraction $f$ of $q_f = nmv_t^3$, the "free-streaming limit." We may, therefore, arbitrarily define an effective heat flow as either $q = \min(q_c, fq_f)$, or $q = q_c/(1 + q_c/fq_f)$,[7] based on the "sharp cutoff" or "harmonic mean" method, respectively. Both methods yield similar results, though the harmonic mean, adopted in this study, gives a stronger reduction for a given value of $f$. Currently acceptable values for $f$ range from about 0.03 to 0.2 (larger values essentially give $q = q_c$).[8] *A priori*, based on the simple arguments presented above, there is no simple way to predict a unique value of $f$. Also, because of its local character, one cannot expect the flux limiter to be applicable in situations where nonlocal transport effects are dominant. In particular, it fails to account for the possibility of preheat.

Although the flux limiter is a very useful tool in many situations, one must exercise caution when using it. As will be demonstrated in the following sections there are certain cases for which it is totally inadequate.

**Heat Flow in a Homogeneous Plasma**

To more accurately investigate nonlocal transport the FP equation must be solved numerically. Our starting assumption is once again the expansion defined by Eq. (2), which is sufficient for demonstrating the major features of nonlocal transport and is probably adequate for most transport problems relevant to ICF.[4] The contributions from other terms in the expansion become necessary when one is interested in nearly collisionless phenomena and electromagnetic instabilities.[13]

We do not assume a Maxwellian form for $f_o$, unlike in the previous section, but rather solve for it using the equation

$$\frac{\partial f_o}{\partial t} + \frac{v}{3}\nabla \cdot \boldsymbol{f}_1 = \frac{1}{v^2}\frac{\partial}{\partial v}\left[\frac{v^2}{3}\boldsymbol{a}\cdot\boldsymbol{f}_1 + Y\left(C_o f_o + D_o \frac{\partial}{\partial v} f_o\right) + \frac{YnZ}{6v} v_o^2 \frac{\partial}{\partial v} f_o\right], \tag{5}$$

where $\boldsymbol{a} = |e|\boldsymbol{E}/m$, $Y = 4\pi(e^2/m)^2 \ln\Lambda$, and $C_o(f_o)$ and $D_o(f_o)$ are integral operators, as defined by Shkarofsky *et al.*[10] The last term in the equation is the inverse-bremsstrahlung operator, with $v_o$ being the electron quiver velocity in the laser field.[14] Equations (3) and (5), coupled with the quasi-neutrality condition and a few modifications to account for ion motion, are solved in the 2-D code SPARK, the details of which are described in Refs. 5 and 6.

As a first illustration of kinetic transport consider a homogeneous plasma of temperature $T_o$, where we apply a perturbation of the form $\delta T(t)e^{ikx}$, such that $\delta T \ll T_o$. Using the energy-conservation equation $(3/2)n\partial_t T + \nabla \cdot \boldsymbol{q} = 0$, it is easily shown that $\delta T_c(t) = \delta T_c(t=0)e^{-t\alpha}$, where $\alpha = 2k^2\kappa_c/3n$ is the classical decay rate. By numerically calculating the temperature decay using SPARK, and defining $\alpha_{FP} = 2k^2\kappa_{FP}/3n$, it is then possible to obtain $\kappa_{FP}/\kappa_c$. This gives us a measure of departure from classical transport. By varying $k$ we obtain different values of $\kappa_{FP}/\kappa_c$, which are then plotted in Fig. 42.2 as a function of $(k\lambda_d)^{-1}$, where $\lambda_d = (\lambda_e\lambda_t)^{1/2} = (Z+1)^{1/2}\lambda_t$ is an effective delocalization length (or stopping length), and $\lambda_e = T^2/4\pi ne^4 \ln\Lambda$ is the energy-loss mean free path.[15] The origin of $\lambda_d$ may be traced back to Eqs. (3) and (5) by estimating

$$v^{-2}\partial(YC_o f_o)/\partial v \sim (v_t/\lambda_e) f_o$$

as the electron-electron energy-loss term, and comparing it to the spatial diffusion term $v\nabla \cdot \boldsymbol{f}_1 \sim v_t\lambda_t\nabla^2 f_o \sim v_t\lambda_t f_o/\lambda_d^2$, assuming $v = v_t$. In effect, $\lambda_d$ provides a better measure of delocalization than $\lambda_t$ alone (with some appropriate weighting to account for the higher-velocity heat-carrying electrons), since it also depends on the strength of the electron-electron energy loss.

In Fig. 42.2 we observe a departure from classical heat flow, in the form of flux inhibition, for scale lengths $k^{-1} < 200\,\lambda_d$. Such an effect, which has been predicted by Bell in the context of ion waves,[16] clearly demonstrates a situation where nonlocal electron transport is present and yet $q_c \ll fq_f$, i.e., the heat flow is unsaturated. In fact, since the heat flow is arbitrarily small, there is no unique value of $f$ that will give $q_{FP} = q_c$. The explanation for the flux inhibition comes from the fact that, for $l \ll 200\,\lambda_d$, the heat-carrying electrons are able to diffuse across many wavelengths, thereby reducing their density gradient in phase space. Since the modulation $e^{ikx}$ refers to the thermal electrons (with energies ~ $T$), and the electron thermalization to higher energies ($E^* \sim 7T$) is not instantaneous, the effective heat flux is reduced, as shown schematically in Fig. 42.3.

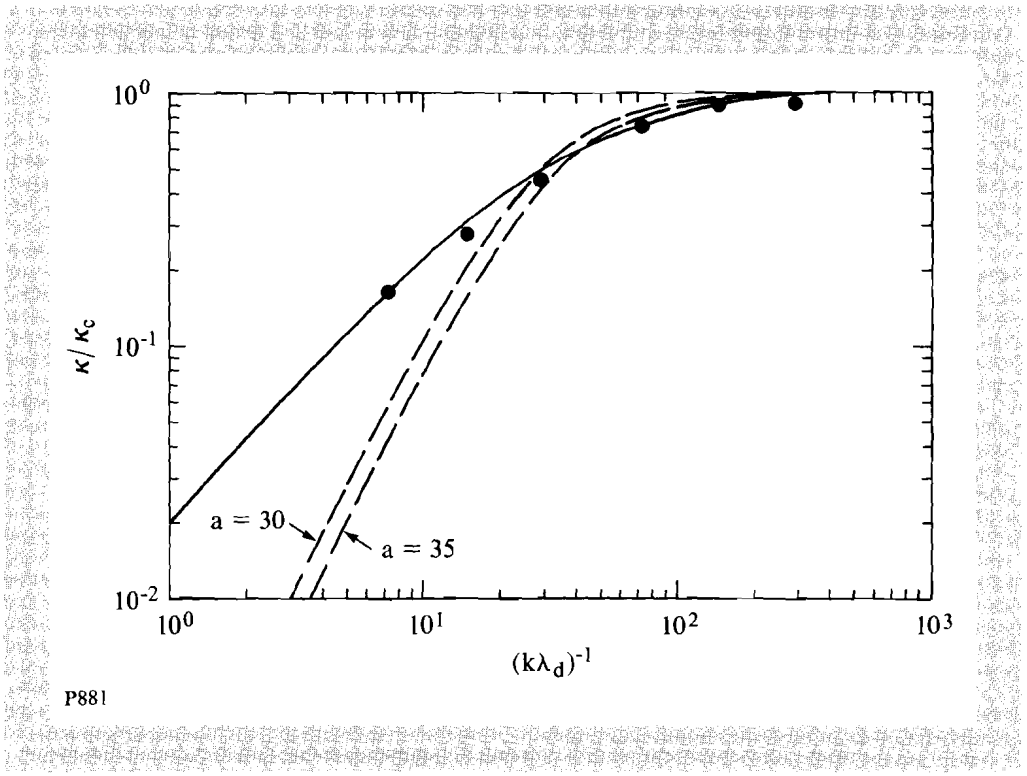


Fig. 42.2
Plot of $\kappa_{FP}/\kappa_c$ (solid curve) and $\kappa_d/\kappa_c$ (dashed curves) as functions of $(k\lambda_d)^{-1}$. Data points are obtained from a 2-D FP simulation.

At this point it is interesting to investigate the properties of so-called delocalization models of heat flux, designed to bridge the gap between fluid and kinetic theories. The simplest one, first proposed by Luciani *et al.*,[15] is given by

$$q_d(x) = \int_{-\infty}^{\infty} dx' \frac{q_c(x')}{2\lambda_0(x')} \exp\left[-|x - x'|/\lambda_0(x')\right]$$

for a homogeneous plasma. Here, $\lambda_0 = a\lambda_d$ and $a$ is a free parameter. By Fourier analyzing the above equation it is straightforward to show that

$$q_d / q_c = \kappa_d / \kappa_c = (1 + a^2 k^2 \lambda_d^2)^{-1}$$

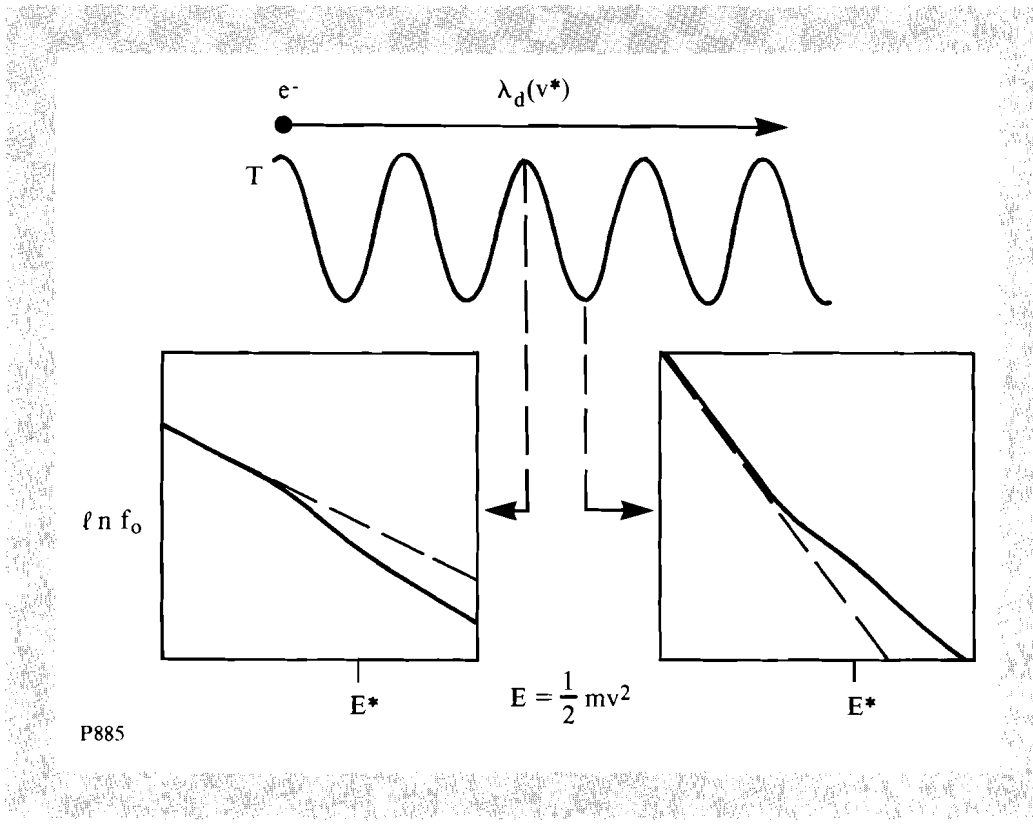


Fig. 42.3
Qualitative description of nonlocal transport. In the distribution plots, solid curves are based on a kinetic calculation, whereas dashed curves are obtained assuming a Maxwellian distribution at the local temperature.

so that at first sight it appears to have the desired property that $\kappa_d/\kappa_c$ decreases for large $k\lambda_d$. However, plotting this function in Fig. 42.2 using $a = 30$–$35$ (which covers the range of values quoted in the literature)[15] gives poor agreement with the FP data. The main reason is that for large $k\lambda_d$, $\kappa_{FP}/\kappa_c \sim (k\lambda_d)^{-1}$, whereas $\kappa_d/\kappa_c \sim (k\lambda_d)^{-2}$. Such a discrepancy may explain the somewhat limited success enjoyed by delocalization models in ICF-related transport simulations.[8,17]

**Heat Flow in a Laser-Heated Plasma**

Here we review the results of 2-D transport simulations that illustrate some of the subtleties associated with nonlocal transport. We investigate the thermal response of a CH target that has been subjected to nonuniform laser irradiation. It is particularly important to predict the level of thermal smoothing at the beginning of the laser pulse since the effectiveness of the implosion may depend on it.

As it is not yet feasible to run a full 2-D laser-ablative implosion using SPARK we restrict ourselves to the early-time response by keeping the ions stationary. The background density profile, shown in Fig. 42.4, is obtained using the 1-D fluid code *LILAC*.[18] The conditions correspond to that of a

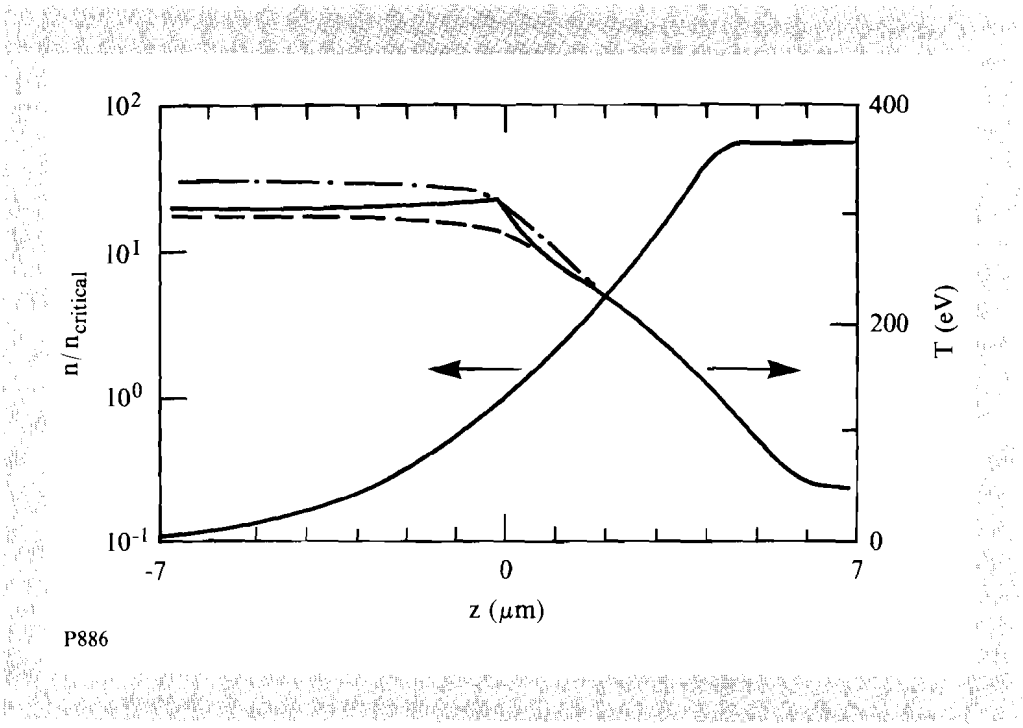


Fig. 42.4
Density $n$ (normalized to the critical density value) and temperature $T$ (in eV) profiles after a 100-ps laser pulse. Curves are identified as in Fig. 42.1.

300-$\mu$m-diameter, 10-$\mu$m-thick CH target irradiated by a 0.35-$\mu$m laser of peak intensity $5 \times 10^{14}$ W/cm$^2$ and a Gaussian temporal pulse of 600-ps FWHM. The plot is taken at 600 ps before the peak, when the intensity is $\sim 3 \times 10^{13}$ W/cm$^2$. SPARK is initialized at this intensity (which is maintained constant in time) and at a temperature of 50 eV. After a few tens of picoseconds the coronal temperature reaches approximately 300 eV and the thermal front evolves in a quasi-steady fashion. Figure 42.4 shows the FP and fluid results at 100 ps. The very slight flux inhibition (not noticeable in the figure) is well modeled by using $f = 0.1$ (harmonic). We note that the coronal temperature increases with flux limitation (as less heat is allowed into the overdense plasma) so that we also obtain better agreement for the laser absorption fraction $\varphi$, i.e., $\varphi_{FP} = 0.74$, $\varphi_c = 0.78$ and $\varphi\,(f = 0.1) = 0.73$. Such a result is typical for simulations with short-wavelength lasers (<1 $\mu$m) at moderate intensities (<$10^{15}$ W/cm$^2$).[4,15]

The above simulation has been repeated by applying a small modulation in the $x$ direction to the incident laser intensity of the form $\sin(kx)$, where $\lambda_\perp = 2\pi/k = 10$ $\mu$m. Figure 42.5 shows the calculated root-mean-square (rms) temperature deviation at 100 ps defined by

$$\sigma = \left\{\left[\int dx (T - \langle T\rangle)^2\right] / \int dx\right\}^{1/2} \langle T\rangle^{-1},$$

where $\langle T \rangle$ is the average temperature. All plots have been normalized to the rms laser intensity. Axial and transverse heat flow, normalized to $q_f$, are shown in Figs. 42.6(a) and 42.6(b), respectively. Here, $q_c$ is calculated using the FP temperature profiles.

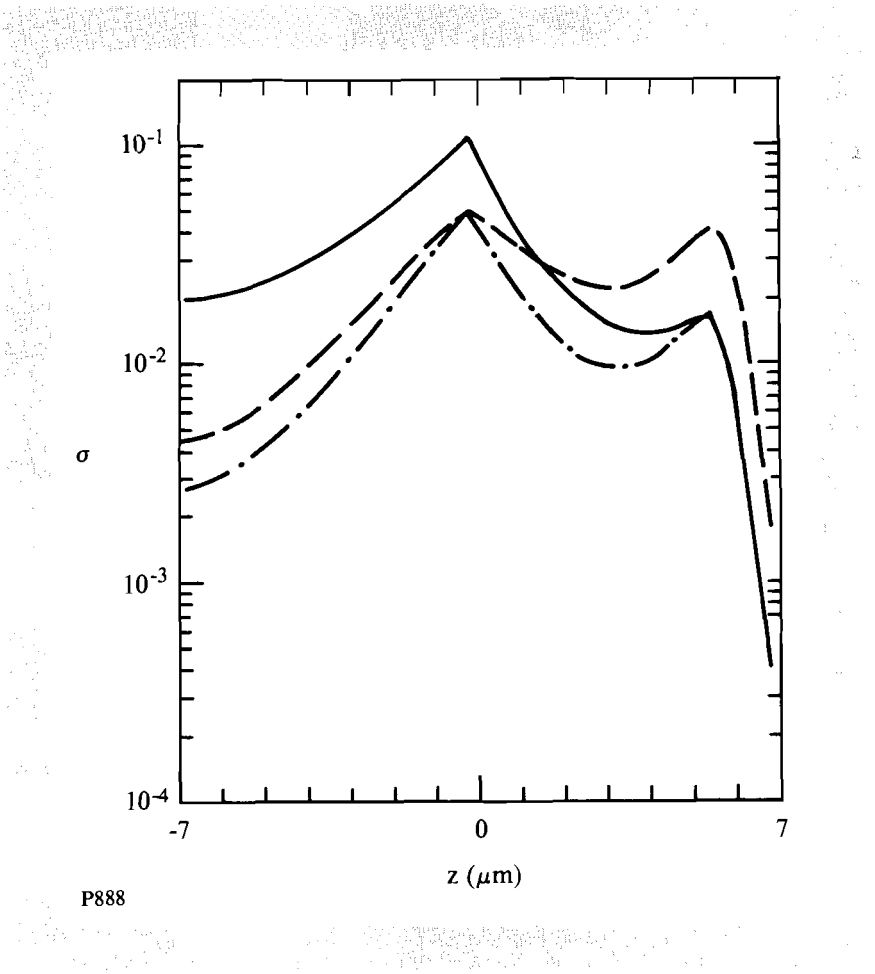


Fig. 42.5
Plot of the rms temperature deviation (normalized to the rms laser-intensity deviation) as a function of $z$. Curves are identified as in Fig. 42.1.

Despite the good agreement between fluid and kinetic results for the 1-D temperature profiles, the same is not true for the transverse spatial modulation. Nonlocal transport gives rise to less smoothing in the corona and an enhancement at higher densities. Both these regimes are now discussed in turn. To characterize the coronal smoothing, the ratio $\sigma_{FP}/\sigma_c$ is calculated at the critical surface and the result is plotted in Fig. 42.7 as a function of $\lambda_\perp$. The increase of $\sigma_{FP}/\sigma_c$ as $\lambda_\perp \to 0$ is a consequence of lateral heat-flux inhibition, of the type discussed in the previous section for the special case of a homogeneous plasma. For a more quantitative demonstration of this effect we first assume that $S \sim ik(q_{FP})_x \sim ik(q_c)_x$ in the corona, where $S$ is the laser energy deposition rate. Using the definition $\kappa_{FP} = -(q_{FP})x/ik\delta T_{FP}$, we find that $\kappa_{FP}/\kappa_c \sim \delta T_c/\delta T_{FP} \sim (\sigma_{FP}/\sigma_c)^{-1}$, allowing us to plot $\kappa_{FP}/\kappa_c$ as a function of $\lambda_\perp/(2\pi\lambda_d)$ in Fig. 42.2 (full circles), where $\lambda_d = 0.75\ \mu$m at the critical surface. This occurrence of reduced coronal thermal smoothing

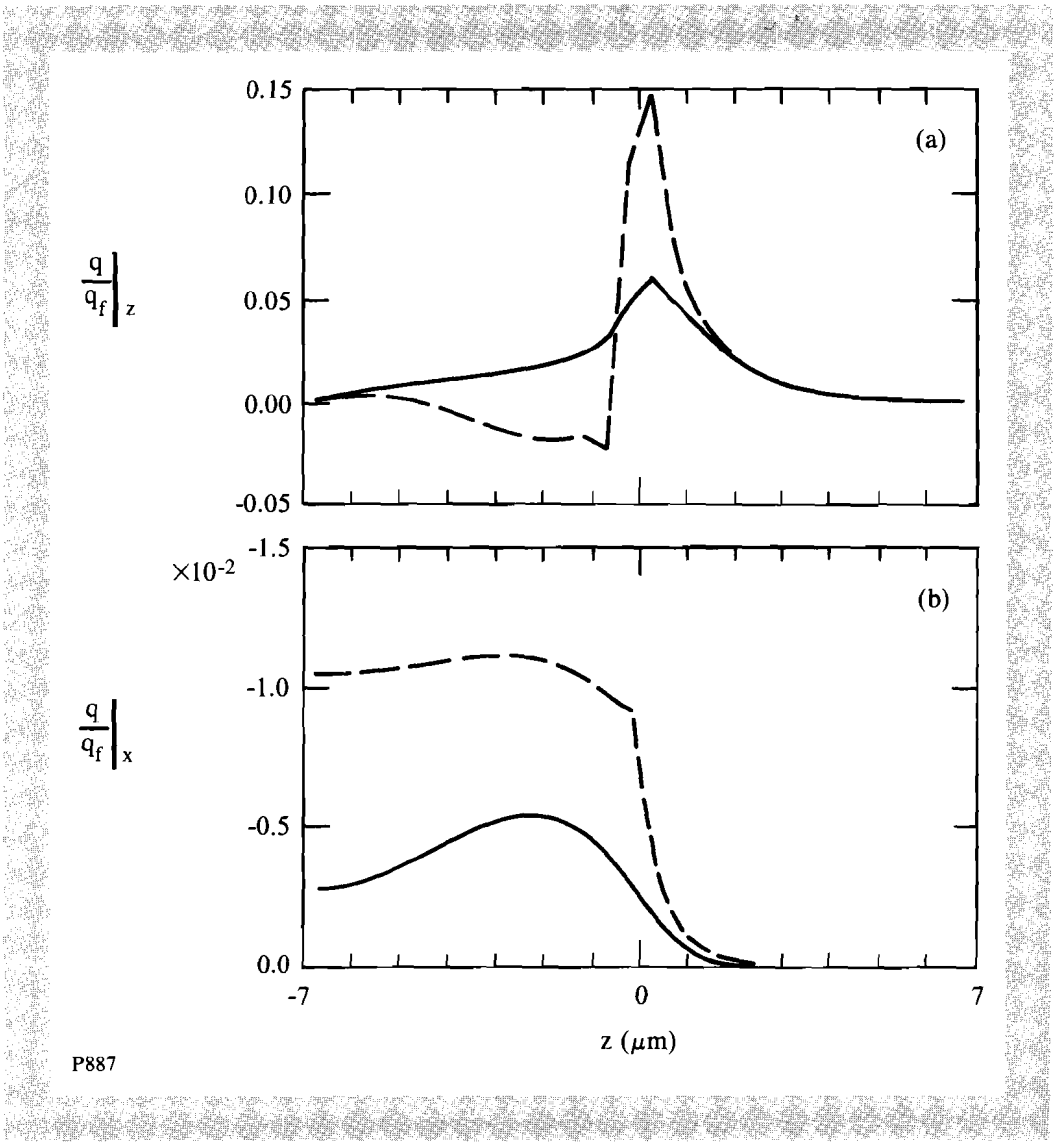


Fig. 42.6
Plot of heat flow (normalized to $q_f$) in the (a) $z$ direction (axial) and in the (b) $x$ direction (transverse) at $x = 0$, as functions of $z$. Here, solid curves refer to $q_{FP}$, whereas dashed curves refer to $q_c$ using FP temperatures.

in longer-scale-length plasmas irradiated by higher intensities has been previously reported by Epperlein *et al.*[5]

The clue for the enhanced smoothing at high densities lies in the axial flux inhibition near critical [see Fig. 42.6(a)]. This acts to reduce the effective flow of thermal modulation away from the critical surface to the overdense plasma. By applying a flux limiter we can reproduce this effect to some extent as shown in Fig. 42.7. The enhancement of lateral thermal smoothing due to axial flux inhibition was first predicted by Skupsky,[19] using a crude steady-state fluid model. More recently Rickard *et al.*[20] used a FP code to predict a large increase in thermal smoothing in the long-wavelength ($\lambda_\perp$)

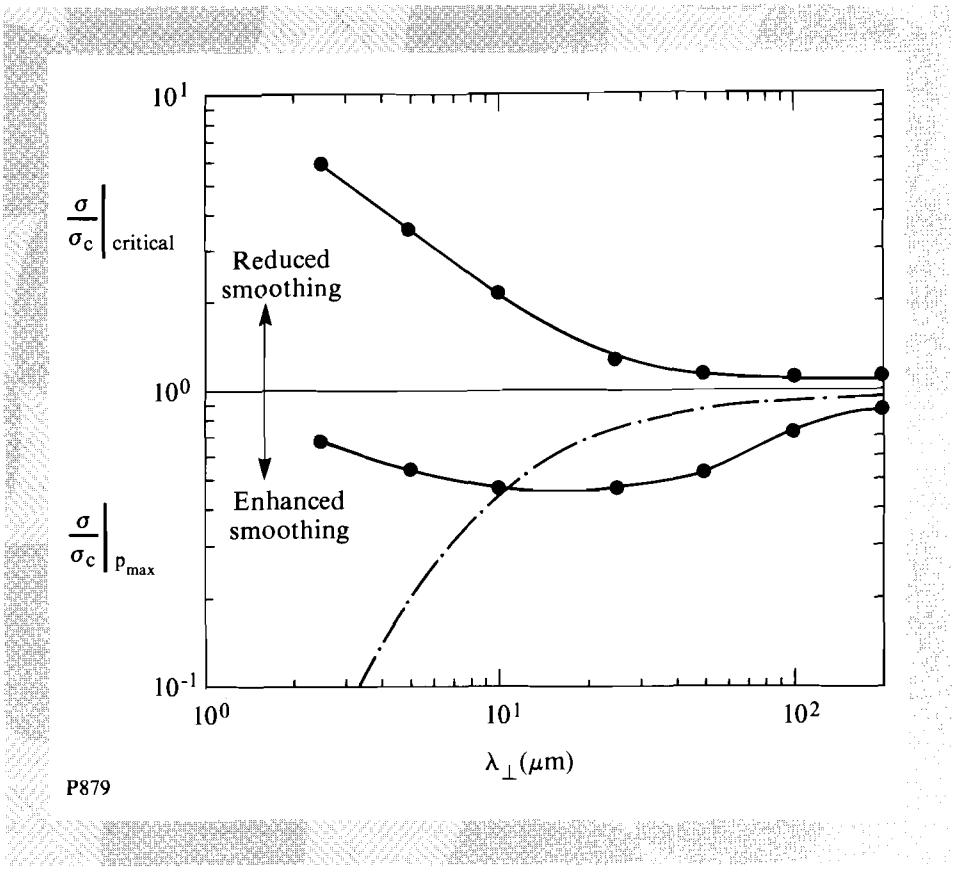


Fig. 42.7
Plot of $\sigma_{FP}/\sigma_c$ (solid curves) and $\sigma^*(f=0.1)/\sigma_c$ (dash-dotted curve) as functions of $\lambda_\perp$ ($\mu$m), calculated at $n_{critical}$ and at maximum pressure.

limit. They used, however, a much higher laser intensity ($10^{15}$ W/cm$^2$) that gave rise to a much stronger axial flux inhibition and hence reduced thermal modulation at high densities. Here we calculate $\sigma_{FP}/\sigma_c$ where pressure is a maximum $p_{max}$ (~4.4 $\mu$m away from the critical surface) and obtain only a modest enhancement in smoothing at large wavelengths, as seen in Fig. 42.5. We do, however, predict that for a wide range of $\lambda_\perp$ (6 $\mu$m – 40 $\mu$m), $\sigma_{FP}/\sigma_c \sim 0.5$, which represents a factor of ~2 improvement in pressure uniformity at $p_{max}$. At smaller wavelengths the reduced lateral smoothing at critical starts to dominate and the value of $\sigma_{FP}/\sigma_c$ increases again. (In practice this is relatively unimportant since at $p_{max}$, we find that $\sigma < 10^{-2}$ for $\lambda_\perp < 6$ $\mu$m.) These effects are not accurately modeled with flux-limited classical transport as shown in Fig. 42.7 by plotting $\sigma(f=0.1)/\sigma_c$.

## Conclusions

Care must be taken when interpreting transport data using flux-limited classical heat conduction. For short-wavelength lasers (<1 $\mu$m) at moderate intensities (<$10^{15}$ W/cm$^2$) a fluid model provides an adequate description of the transport under uniform illumination conditions. A modest amount of flux limitation ($f \sim 0.1$) is then sufficient to fine tune the results. However,

one must be aware that classical transport (flux limited or otherwise) cannot model preheat because of the long-mean-free-path electrons. In the FP simulations presented here this issue was not addressed satisfactorily because of the relatively high initial plasma temperatures. Mima *et al.*[21] have recently shown, using a 1-D FP code coupled to a Lagrangian fluid solver, that preheat can significantly degrade the performance of thin low-$Z$ shell targets irradiated by 0.53-$\mu$m laser light. The magnitude of this effect is expected to be less for shorter-wavelength lasers, by virtue of the higher collisionality of the plasma, though the exact extent remains to be investigated.

When simulating 2-D transport, which may arise as a result of nonuniform laser irradiation, nonlocal effects can drastically alter the results, even when the average 1-D transport appears well modeled by fluid theory. The main consequences of nonlocal transport are given as follows:

1. A severe reduction in the coronal thermal smoothing for spatial modulations less than about 200 $(Z + 1)^{1/2}\lambda_t$.

2. An enhancement in the smoothing at high densities, especially near the pressure maximum, for all spatial modulations.

The first consequence is well explained in terms of flux inhibition of short-scale modulations in a homogeneous plasma. Its main impact would be to reduce the threshold for thermal self-focusing instabilities[22] or any other instabilities that rely on coronal temperature modulations.

The second result arises from the axial flux inhibition from the critical density to higher densities, which acts to reduce the propagation of thermal modulations. The scaling of this phenomenon with plasma and laser conditions has not been fully investigated, nor has the issue of hydrodynamic feedback been addressed. However, the simulations presented here suggest the possibility of a two-fold increase in smoothing (when compared with classical heat-flow modeling) over a wide range of modulation wavelengths. Such an outcome is potentially very beneficial to ICF since, for a given nonuniformity in the incident laser, it predicts a smoother ablation pressure and less chance for seeding hydrodynamic instabilities.

## ACKNOWLEDGMENT

This work was supported by the U.S. Department of Energy Division of Inertial Fusion under agreement No. DE-FC03-85DP40200 and by the Laser Fusion Feasibility Project at the Laboratory for Laser Energetics, which has the following sponsors: Empire State Electric Energy Research Corporation, New York State Energy Research and Development Authority, Ontario Hydro, and the University of Rochester.

## REFERENCES

1. J. Nuckolls, L. Wood, A. Thiesen, and G. Zimmerman, *Nature* **239**, 139 (1972).
2. L. Spitzer, Jr. and R. Härm, *Phys. Rev.* **89**, 977 (1953).
3. D. R. Gray and J. D. Kilkenny, *Plasma Phys.* **22**, 81 (1980).

4. A. R. Bell, R. G. Evans, and D. J. Nicholas, *Phys. Rev. Lett.* **46**, 243 (1981); J. P. Matte and J. Virmont, *ibid.* **49**, 1936 (1982); J. R. Albritton, *ibid.* **50**, 2078 (1983); T. H. Kho, D. J. Bond, and M. G. Haines, *Phys. Rev. A* **28**, 3156 (1983); J. P. Matte, T. W. Johnston, J. Delettrez, and R. L. McCrory, *Phys. Rev. Lett.* **53**, 1461 (1984); J. F. Luciani, P. Mora, and R. Pellat, *Phys. Fluids* **28**, 835 (1984); A. R. Bell, *ibid.* **28**, 2007 (1985); and S. Jorna and L. Wood, *J. Plasma Phys.* **38**, 317 (1987).

5. E. M. Epperlein, G. J. Rickard, and A. R. Bell, *Phys. Rev. Lett.* **61**, 2453 (1988).

6. E. M. Epperlein, G. J. Rickard, and A. R. Bell, *Comput. Phys. Commun.* **52**, 7 (1988); G. J. Rickard, A. R. Bell, and E. M. Epperlein, *Phys. Rev. Lett.* **62**, 2687 (1989).

7. R. C. Malone, R. L. McCrory, and R. L. Morse, *Phys. Rev. Lett.* **34**, 721 (1975).

8. J. Delettrez, *Can. J. Phys.* **64**, 932 (1986).

9. W. L. Kruer, *The Physics of Laser Plasma Interactions* (Addison-Wesley, Redwood City, CA, 1988).

10. I. P. Shkarofsky, T. W. Johnston, and M. P. Bachysnky, *The Particle Kinetics of Plasmas* (Addison-Wesley, London, 1966).

11. E. M. Epperlein and M. G. Haines, *Phys. Fluids* **29**, 1029 (1986).

12. D. Shvarts, J. Delettrez, R. L. McCrory, and C. P. Verdon, *Phys. Rev. Lett.* **47**, 247 (1981).

13. E. M. Epperlein, *Plasma Phys. & Controlled Fusion* **27**, 1027 (1985).

14. A. B. Langdon, *Phys. Rev. Lett.* **44**, 575 (1980).

15. J. F. Luciani, P. Mora, and J. Virmont, *Phys. Rev. Lett.* **51**, 1664 (1983); J. R. Albritton, E. A. Williams, I. B. Bernstein, and K. P. Swartz, *ibid.* **57**, 1887 (1986); P. A. Holstein, J. Delettrez, S. Skupsky, and J. P. Matte, *J. Appl. Phys.* **60**, 2296 (1986).

16. A. R. Bell, *Phys. Fluids* **26**, 279 (1983).

17. M. K. Prasad and D. S. Kershaw, *Phys. Fluids B* **1**, 2430 (1989).

18. J. Delettrez (private communication).

19. S. Skupsky, LLE Report **131** (1982).

20. G. J. Rickard, I. R. G. Williams, and A. R. Bell, presented at the 19th Annual Anomalous Absorption Conference, Durango, CO, June 1989.

21. K. Mima *et al.*, *Laser and Part. Beams* **7**, 487 (1989).

22. E. M. Epperlein, presented at the 19th Annual Anomalous Absorption Conference, Durango, CO, June 1989.